System-Inherent Grid Synchronous Stability Boundary and Spontaneous Synchronization

Yu Yuan *

Posted Date: 28 October 2023

doi: 10.20944/preprints202310.1791.v1

Keywords: Power system; spontaneous synchronization; synchronous stability boundary

Article

System-Inherent Grid Synchronous Stability Boundary and Spontaneous Synchronization

Yu Yuan

SICHUAN TECHNOLOGY & BUSINESS COLLEGE; yuyuan.sctbc@outlook.com

Abstract: Synchronization is a prerequisite for the stability of electrical energy, which is the cornerstone of a functioning society[1]. Identifying whether generators are synchronized or not has been attracting immense research interest. Utilizing synchronized stability boundaries can strongly simplify stability discrimination. However, fundamental issues such as determining accurate stability boundaries remain challenging[2,3]. In this study, an accurate synchronized stability boundary equation that is independent of the system and disturbances is presented, and it is applicable to an arbitrarily coupled grid. The special structure induced by spontaneous synchronization appears to be only near the stability boundary. The results of this study show that: the synchronous stability boundary is an intrinsic property of the system, independent of its structure and parameters. Synchronization on the network may be independent of the network. These conclusions will challenge the traditional perception of synchronization on networks, and the synchronization stability of the grid can be analyzed in a uniform way.

Keywords: power system; spontaneous synchronization; synchronous stability boundary

Introduction

Synchronous stability is a prerequisite for the normal operation of a power grid[4]. The loss of stability in a power system can cause power supply disruptions for a wide range of customers. Large power systems are complex coupled systems where uncertainties[5] and nonlinearities coexist. In the stability analyses of power grids, a high level of real-time performance is required[6]. To analyze the stability of these systems, researchers have developed numerous insightful stability discriminatory methods[7–12], including finding stability regions and their boundaries[2,3,13].

Finding the stability boundary of a system is an important fundamental problem[3,14,15]. The boundary, which can be used to strongly simplify stability discrimination, is the union of unstable equilibrium points (UEPs)[16]. When an operating point is outside the boundary, the corresponding system is unstable[13]. The synchronous stability boundary, which is a core concept of grid stability, is closely related to many issues[6,17,18]. Therefore, studying synchronous stability boundaries has a significant impact on the development of power systems. For decades, scientists and engineers have wanted to find an analytical equation to describe the boundary[2,3,19]. However, researchers continue to face challenges, such as high computational complexity, difficulty of visualization, and difficulty in adapting to system uncertainty.

In addition, network concepts have been utilized to explain the synchronization of generators by studying the spontaneous synchronization conditions of various networks[20]. However, the reasonableness of this assumption, which directly equates the spontaneous synchronization with the synchronization stability, has been questioned[9,21] and challenges remain in applying it to real networks[8]. One way to clarify this debate is to obtain data through traditional power system research methods and to obtain evidence of spontaneous synchronization from them. However, such results are rarely reported[9]. Electrical engineering communities need an explanation with clearer physical meaning.

Here, a simple equation based on a coordinate transformation and new concepts was derived and visualized to describe the stability boundary of a power system. The derivation of the equation

Preprints (www.preprints.org) | NOT PEER-REVIEWED | Posted: 28 October 2023 doi:10.20944/preprints202310.1791.v1

is based entirely on physically based concepts. The form of the equation is independent of the network topology, component parameters and fault disturbances and is therefore very generalizable. At the same time, the synchronization stability boundary represented by the equation is independent of the network and the perturbations. This equation can be used to analyze the synchronization stability of the grid in a uniform way. The critical clearing time (CCT) and the generator critical rate were calculated by fitting the disturbed trajectory using the same variable system as the boundary. Additionally, simulation results on fine scales from the IEEE standard arithmetic models demonstrated evidence of spontaneous synchronization[1], which occurred near the synchronization stability boundary. This result may also hint that synchronization on the network may be independent of the network. This will challenge the traditional perception of synchronization in networks. Directly discriminating synchronization on the network will be simplified to the relationship between the network and the operating point coordinates. Determining the stability of a coupled grid containing n generators requires only n pairs of variables. These variables have a clear physical meaning and are easily accessible. Spontaneous synchronization and synchronous stability have been widely discussed in many fields[8,20]. In this case, for potential scenarios where it is difficult to construct a network model, the study demonstrates the success of directly determining synchronization on the network.

Schematic diagram of basic concepts

The generator variables are selected from the port bus voltage per unit U and the rotor speed per unit ω, $U \in [0,+\infty)$, $\omega \in (-\infty,+\infty)$. The coordinates of ω are transformed: $\delta_\omega = 2\arctan(\omega), \delta_\omega \in (-\pi,\pi)$, where δ_ω is the angle of rotation rate. The angle of rotation rate of the *i*th generator δ_{ω_i} is abbreviated as δ_i in the following. Note: δ_ω is not the power angle.

a. Synchronised system operation before disturbance, $\omega_1 = \omega_2 = \cdots = \omega_n = 1$ and $\delta_i = 2\arctan(\omega_i) = \frac{\pi}{2}, i = 1,2,\cdots,n$. The magenta dot indicates the operating point of the generator: (U, δ_ω).

b. The angle of rotation rate of the subsystems differ after the disturbance. u_K, u_L are the per unit voltage of the port bus of the Kth and Lth generators, respectively, $\delta_{KL} = |\delta_K - \delta_L| \geq 0$ is the difference in the angle of rotation rate between the Kth and Lth generators. Δu is defined as the coupling potential difference between generators Kth and Lth (yellow dotted line between Cyan dots). Correspondingly, u' is constructed to describe the synchronous potential difference between generators Kth and Lth (solid blue line between magenta square dots). The set of points where $|u'| = |\Delta u|$ is the synchronous stability boundary (see Methods for details: Derivation of the boundary equations).

Materials and Methods

Extensive interconnections between generators would make stability analysis very difficult(see Extended Data Figure 1). To solve this problem, the concept of a meta-generator is introduced here. At moment t, the instantaneous values of the n generators system $(U_i'(t), \delta_i'(t)), i \in (1,2,...,n)$ are arranged in descending order by δ_ω, relabelled, and then reconstituted as the n meta-generator system $(u_i(t), \delta_i(t)), i \in (1,2,...,n)$.

Preprints (www.preprints.org) | NOT PEER-REVIEWED | Posted: 28 October 2023 doi:10.20944/preprints202310.1791.v1

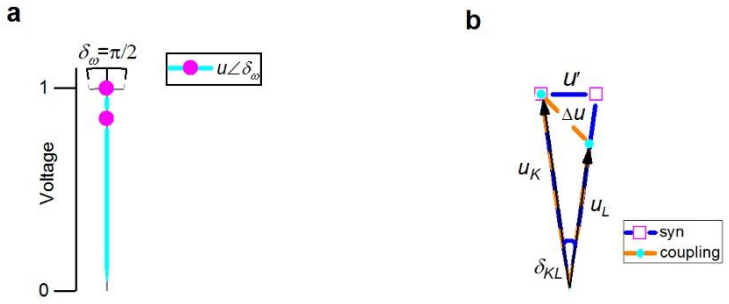

Figure 1. Schematic diagram of the power system operating coordinate system (U,δ_ω).

The essence of the connection between the meta-generators and the original generators is the permutation: $S=\begin{pmatrix}\delta_1' & \delta_2' & \dots & \delta_i' & \delta_{i+1}' & \dots & \delta_n'\\ \delta_1 & \delta_2 & \dots & \delta_{i+1} & \delta_i & \dots & \delta_n\end{pmatrix}$. When the condition $\delta_{i+1}'(t)>\delta_i'(t)$ holds, $(u_{i+1}(t),\delta_{i+1}(t))=(u_i'(t),\delta_i'(t)),(u_i(t),\delta_i(t))=(u_{i+1}'(t),\delta_{i+1}'(t))$.

Define the distribution matrix H, where $H_{i'j}$ is the share of the i'th generator in the jth meta-generator in period T. H can be a potential choice for generator coherent group prediction techniques.

Data sources and experimental procedures

In this study, the IEEE 39-BUS and IEEE 9-BUS models (Extended Data Figures 4–6) were used. The two models are simulated separately using a simulation software package. Here, the fault was set as a three-phase short circuit to ground. The disturbed operating point of each generator was calculated. To observe the movement pattern of the disturbed operating points, no parameters were set for the control elements .

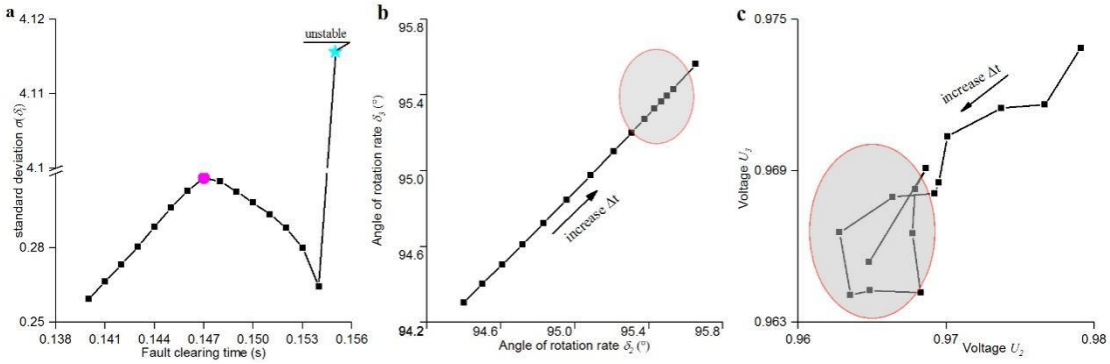

Figure 4. Boundary effects of the 18bus three-phase short circuit to ground fault, with increased fault duration Δt from 0.140s to 0.154s ($d(\Delta t)=0.001s$), and the trajectory of the disturbed operating point near the boundary. The arrow shows the direction of increase of Δt. The simulation result showed instability at Δt =0.155s.

In advance, the fault location was fixed, and the fault duration Δt was set. This experiment simulated the rotation rate $\omega_i'(t)$ and port bus voltage $u_i'(t)$ of the ith generator after different disturbances. Then, the angle of rotation rate of the ith generator $\delta_i(t)$ was calculated. Δt was increased in a fixed step length and $u_i'(t)$, $\delta_i(t)$ were calculated again until the system was destabilised. The faulty position was replaced, and the above steps were repeated.

Preprints (www.preprints.org) | NOT PEER-REVIEWED | Posted: 28 October 2023 doi:10.20944/preprints202310.1791.v1

Subsequently, $(u_i'(t),\delta_i'(t)), i\in(1,2,...,n)$ was arranged and relabelled as $(u_i(t),\delta_i(t)), i\in(1,2,...,n)$. This was then averaged as follows:

The mean of $(u_i(t),\delta_i(t)), i\in(1,2,...,n)$ over $[0,T]$ was found: $u_i=\frac{1}{T}\int_0^T u_i(\tau)d\tau$ and $\delta_{KL}=\frac{1}{T}\int_0^T \delta_{KL}(\tau)d\tau=\frac{1}{T}\int_0^T \left|\delta_K(\tau)-\delta_L(\tau)\right|d\tau=\frac{1}{T}\int_0^T \delta_K(\tau)-\delta_L(\tau)d\tau=\delta_K-\delta_L$.

The mean of $(u_i(t),\delta_i(t)), i\in(1,2,...,n)$ over $[T_m,T_m+dT]$ was also found: $\delta_i(t_m)=\frac{1}{dT}\int_{T_m}^{T_m+dT}\delta_i(\tau)d\tau, U_i(t_m)=\frac{1}{dT}\int_{T_m}^{T_m+dT}U_i(\tau)d\tau, \delta_{kl}(t_m)=\delta_k(t_m)-\delta_l(t_m)$ There are several definitions of mean, and the simplest, i.e., the arithmetic mean, was used here.

This work added adjacent meta-generator data (u_K,u_L,δ_{KL}) and $(u_K(t_m),u_L(t_m),\delta_{KL}(t_m))$ to the coordinate system $u_K-u_L-\delta_{KL}$ to assess the system stability (Figure 2.b) and time intervals of instability (T_m,T_m+dT) (Figure 2.d).

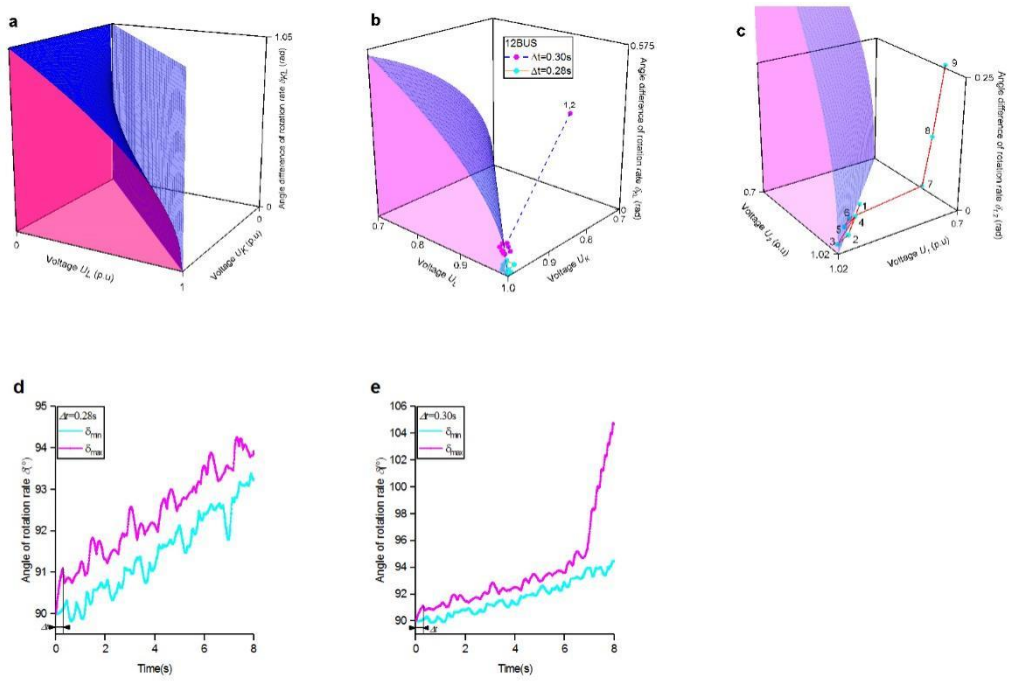

Figure 2. Stability boundary.

An expression was fitted with Δt as the independent variable and $u_K,u_L,\delta_K,\delta_L,\delta_{KL}$ as the dependent variable (Figure 3). CCT and UEP were then calculated.

Preprints (www.preprints.org) | NOT PEER-REVIEWED | Posted: 28 October 2023 doi:10.20944/preprints202310.1791.v1

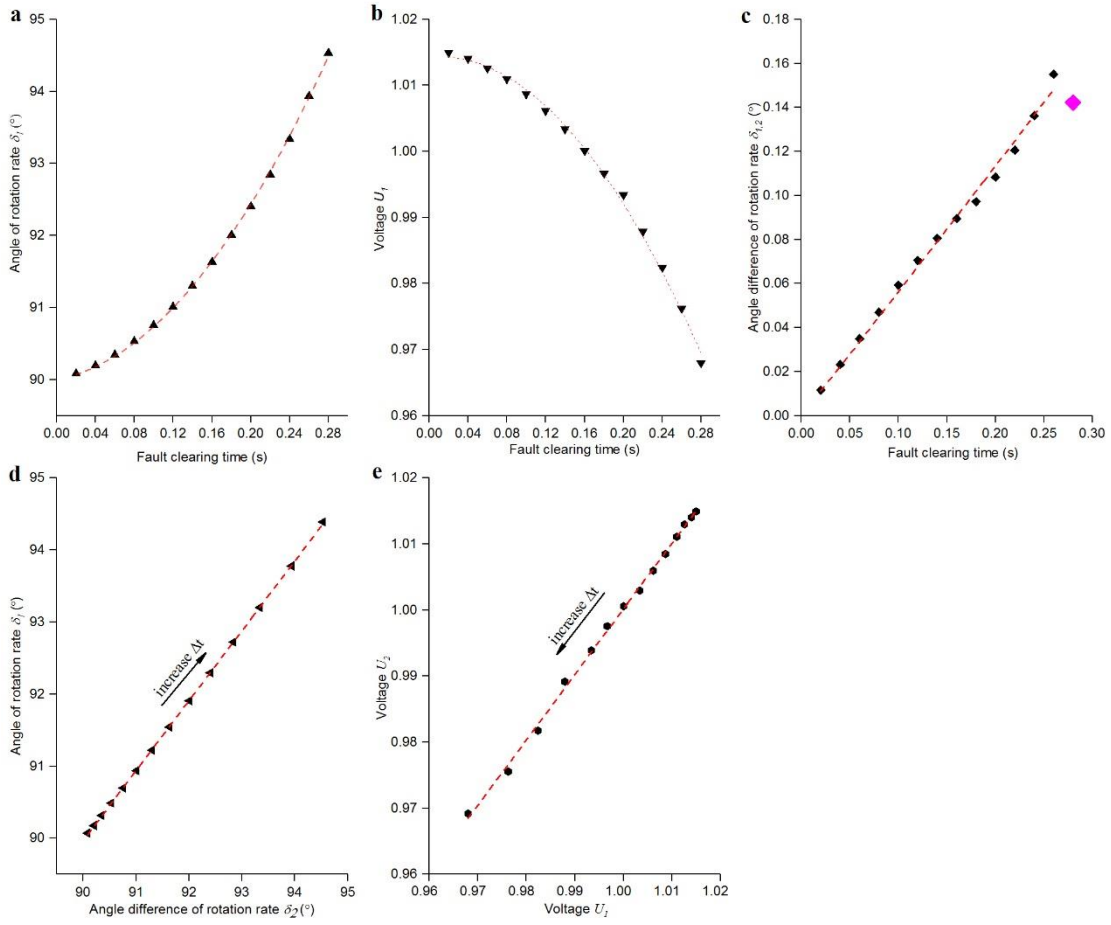

Figure 3. Fitting results for perturbed trajectories of a 12BUS trajectory of disturbed operating points after a three-phase short circuit to ground fault. In the expressions, (i) denotes the ith meta-generator, and $i=1,\cdots,k,l,\cdots,n$. The subscripts u and ω denote the coefficients of the meta-generators at $u_i-\Delta t$ and $\delta_i-\Delta t$, respectively. $\Delta T'$ is the starting fault duration at which self-organised behaviour occurs at the disturbed operating point. To make it easier to show the details, δ_{kl} in the picture uses the angle system.($d(\Delta t)=0.02s$).

Near the boundary, $\sigma(\delta_i),\delta_i,u_i$ was calculated at a finer scale.

Derivation of the boundary equation

As shown in Figure 1, $\Delta u=\sqrt{u_k^2+u_l^2-2u_ku_l\cos\delta_{kl}}$, $u'=\sqrt{2u_k^2(1-\cos\delta_{kl})}$.

Following the form of power in electricity $P=\frac{U^2}{R}$, the coupling power $P_{\Delta u}=\frac{|\Delta u|^2}{|Z_{KL}|}$ is defined to characterise the coupling between the meta-generators. To describe the energy required for the generator to maintain synchronous stability, the synchronous power is constructed: $P_{u'}=\frac{|u'|^2}{|Z_{KL}|}$. Z_{KL} is the impedance between the Kth and Lth meta-generators.

When the system is synchronized, the meta-generators are not in balance and are still coupled ($\delta_{KL}=0,u'=0,\Delta u=u_K-u_L\neq 0$). When the system is disturbed, δ_{KL} increases from 0, u' increases from 0, and Δu changes. When the coupling power between the two meta-generators is

Preprints (www.preprints.org) | NOT PEER-REVIEWED | Posted: 28 October 2023 doi:10.20944/preprints202310.1791.v1

sufficient to provide synchronous power, i.e., $|P_{u'}| \le |P_{\Delta u}|$, the system is synchronous and stable. Conversely, when $|P_{u'}| > |P_{\Delta u}|$, there is not enough coupling power to maintain synchronization, and the system is unstable. It is observed that $\frac{|P_{u'}|}{|P_{\Delta u}|} = 1 \Leftrightarrow \frac{|u'|}{|\Delta u|} = 1$.

In summary, $f(u_K, u_L, \delta_{KL}) = \frac{|u'|}{|\Delta u|} = 1$ is the system stability boundary equation. When $\frac{|u'|}{|\Delta u|} < 1$, the system is stable. When $\frac{|u'|}{|\Delta u|} > 1$, the system is unstable. Geometrically, $f(u_K, u_L, \delta_{KL}) = 1$ describes a curved surface that, together with $(0, u_L, \delta_{KL}), (u_K, 0, \delta_{KL}), (u_K, u_L, 0)$, encloses a stable domain. In summary, the boundary equation $|u_K| = |u_L| \cup \frac{|u_L|}{|u_K|} = 2\cos\delta_{KL} - 1$ can be found, where $|u_K| \ge |u_L| \ge 0, \delta_{KL} \in [0, \frac{\pi}{3}]$. The coordinate system $u_K - u_L - \delta_{KL}$ is established, and the boundary is visualized(Figure 2).

Fitting of operating points to trajectories

The intersection of the disturbed trajectory with the stability boundary is the unstable equilibrium point (UEP), and the failure time of the operating point along the disturbed trajectory to reach the UEP is the CCT. To calculate these important results, it is necessary to fit the disturbed trajectory to the kinematic expression in the (u, δ_ω) coordinate system. The variables of the operating point obtained from the simulation are fed into commercial software to fit the expression of the disturbed operating point.

Operating point behaviour on the boundary

$\frac{d\delta_{KL}}{d(\Delta t)}$ is the derivative of δ_{KL} of the meta-generators with respect to Δt. Near the boundary, the derivative of $\frac{d\delta_{KL}}{d(\Delta t)}$ of the partial meta-generators changes from positive to negative (Figure 3). For this unusual phenomenon, on a finer scale, $(u_i(t), \delta_i(t)), i \in (1, 2, ..., n)$ is calculated sequentially for different Δt. The standard deviation of δ_i is calculated separately (Figure.4):

$$\sigma(\delta_i) = \sqrt{\frac{\sum_{i=1}^{n} (\delta_i - \mu(\delta_i))^2}{n}}, \mu(\delta_i) = \frac{\sum_{i=1}^{n} \delta_i}{n}.$$

Result and discuss

Stability boundary

a. Visualisation of the stable boundary. The stability boundary (blue surface) and $(0, u_l, \delta_{kl}), (u_k, 0, \delta_{kl}), (u_k, u_l, 0)$ (pink surface) together enclose the stability domain. The boundary equation is $|u_k| = |u_l| \cup \frac{|u_l|}{|u_k|} = 2\cos\delta_{kl} - 1$ (see Methods for details: Derivation of the boundary equations). For visualisation purposes, the radian system is used for δ_{kl} in the figure.

Preprints (www.preprints.org) | NOT PEER-REVIEWED | Posted: 28 October 2023 doi:10.20944/preprints202310.1791.v1

b and c are the results of the 12BUS three-phase short circuit to ground simulation, respectively. The system is stable at $\Delta t = 0.28s$, unstable at $\Delta t = 0.3s$, and unstable in $(6s,7s)$.

d. Boundary stability results for the 12BUS three-phase short circuit to ground, where Δt is the duration of the fault. The positions of all operating points at $\Delta t = 0.28s$ and $\Delta t = 0.3s$ are indicated by cyan and magenta dots, respectively. The plane $|u_l| = |u_k|$ perpendicular to $u_k - u_l$ is not shown. At $\Delta t = 0.28s$, all the operating points are clustered together. However, $\Delta t = 0.3s$, the operating points are far away from the other points and outside the boundary.

e. The instability process of Multiswing for the 12BUS three-phase ground fault, where $\Delta t = 0.3s$. Numbers 1 to 9 indicate period T_m after the fault, and $dT = 1s$ (see Methods for details). The system is destabilised in the time interval $(6s,7s)$(Figure 2). The diagram shows the operating points of the meta-generators 1 and 2. The operating point crosses the boundary at the time of instability, and δ_{kl} rapidly increases after the voltage changes .

Regarding the synchronization stability, one different assumption,which appears parallel to the Kuramoto model[8], than before [18]: the system requires the synchronous power $P_{u'} = \frac{|u'|^2}{|Z_{KL}|}$ to maintain synchronous stability, and the synchronous power is provided by the coupling power $P_{\Delta u} = \frac{|\Delta u|^2}{|Z_{KL}|}$ within the system, Z_{KL} is the impedance between the Kth and Lth meta-generators. (see Supplementary Materials for details).

$$|u_K| = |u_L| \cup \frac{|u_L|}{|u_K|} = 2\cos\delta_{KL} - 1, |u_K| > |u_L| \geq 0, \delta_{KL} \in \left[0, \frac{\pi}{3}\right] \quad (1)$$

Eq.1 is the analytical equation for the synchronous stability boundary. Specifically, when $\delta_{KL} > 0$, the set where $|u_L| = |u_K|$ is the isolated stability domain. There has been previous research on the isolated domain[2]. Since it is very difficult to always maintain $|u_L| = |u_K|$ after a disturbance of the system, this situation is not discussed in this paper.

In contrast to previous reports[2,3,20], here, The synchronous stability boundary described by Eq.1 is independent of the network topology, system parameters, perturbations and the number of the subsystem. It is an inherent property of the grid systems. Regardless of the changes in the network structure and component parameters, it is only the operating points of the system that change rather than the stability boundary. This feature increases the applicability of the boundary equation to different grid systems and allows the stability of multimachine systems to be analyzed even in scenarios where the topology and parameters are not clear[22], such as in a black box situation. Thus, the synchronization stability of the grid can be analyzed in a uniform way. This has been validated on different standard arithmetic models (Figure 2 and Extended Data Figure 4). Eq.1 is also suitable for identifying the stability of a power system with multiple swings[23] and showing the time interval of instability(as in Figure 2c and e).

Eq.1 has a variant as follows:

$$\delta_{KL}^{cr} = \arccos\left(1 - \frac{|u_K| - |u_L|}{2|u_L|}\right) \quad (2)$$

Preprints (www.preprints.org) | NOT PEER-REVIEWED | Posted: 28 October 2023 doi:10.20944/preprints202310.1791.v1

When $|u_K|, |u_L|$ are sufficiently close[24], the stability margin of the Kth and Lth generator angle rate difference δ_{KL}^{cr} also tends to 0. This indicates that the system may already be in a critical state during normal operation. In this case, even if the difference in the values between δ_K and δ_L is small, it takes only a very small perturbation to make the system unstable[25,26]. This may explain why some systems with very small speed differences are more likely to lose synchronization than those with much larger speed differences.

Placing the calculated or measured operating points in the coordinate system $u_K - u_L - \delta_{KL}$ can help directly determine whether the system is stable. A system is considered unstable as long as at least one point (u_K, u_L, δ_{KL}) is outside the boundary (Figure 2b) and far from the other operating points ($\sigma_{\Delta t}(\delta_i) >> \sigma_{\Delta t-\varepsilon}(\delta_i), 0 < \varepsilon < \Delta t$, where Δt is the fault duration) (Figure 2b and Figure 4a). To determine the stability of a power system of n generators, only n pairs of variables $u_i, \delta_i, i \in (1,2,...,n)$ are needed, which are physically meaningful and easily obtainable.

As one of the concepts closely related to stability, intentional isolation is an effective way of avoiding widespread blackouts following instability[27]. Identifying coherent generators is a prerequisite for building intentional islands[28]. Information regarding the coherence meta-generator groups can be obtained directly from the graph. That is, the partial synchronization of multiple generators, such as chimeric states[29–31], can also be identified with a stable boundary. m operating points outside the boundary indicate that the n meta-generators are sequentially divided into m+1 coherent groups.

Disturbed trajectory and parameters

To understand the behavior of the power system after a disturbance and to calculate the CCT and UEP, it is necessary to study the perturbation trajectories consisting of running points.

a. The projection of the disturbed trajectory in the $\delta_1 - \Delta t$ plane, fitted using the equation $\delta_i = \frac{a_\omega(i)}{2} * \Delta t^2 + b_\omega(i) * \Delta t + c_\omega(i), \Delta t \in (0, \Delta T']$.

b. The projection of the disturbed trajectory in the $u_1 - \Delta t$ plane, fitted using the equation $u_i = \frac{a_u(i)}{2} * \Delta t^2 + b_u(i) * \Delta t + c_u(i), \Delta t \in (0, \Delta T']$.

c. The projection of the disturbed trajectory in the $\delta_{1,2} - \Delta t$ plane, fitted using the equation $\delta_{kl} = \delta_k - \delta_l = a_{kl} * \Delta t^2 + b_{kl} * \Delta t, \Delta t \in (0, \Delta T']$. Notably, $\delta_{1,2}$ descended at $\Delta t = 0.28s$.

d. The projection of the disturbed trajectory in the $\delta_1 - \delta_2$ plane, fitted using the equation $\delta_k = a_\delta * \delta_l + b_\delta, \Delta t \in (0, \Delta T']$, where $\delta_k > \delta_l, a_\delta > 1$.

e. The projection of the disturbed trajectory in the $u_1 - u_2$ plane, fitted using the equation $u_k = a_v * u_l + b_v, \Delta t \in (0, \Delta T']$.

Figure 3.a and 3.b show that the operating points move with a uniformly variable speed before the system becomes unstable.

Contrary to intuition[32], δ_{12} suddenly dropped at $\Delta t = 0.28s$ (Figure 3c). This anomaly suggested that the system appears to have a tendency to maintain its own stability.

Figure 3.d and E show that the perturbed trajectories of the subsystems of the coupled system are linearly correlated in the stability domain. This indicates that for a determined power grid, each

Preprints (www.preprints.org) | NOT PEER-REVIEWED | Posted: 28 October 2023 doi:10.20944/preprints202310.1791.v1

perturbed trajectory has the same T_i', T_i' being the global invariant of the system. The effects of perturbations are global, reflecting the challenges of controlling the stability of complex systems[33–35].

When a high degree of accuracy of the results is not needed, $a_{KL}=0$. The following expression can be derived:

$$\Delta T'=\frac{2\left[b_{KL}-(a_\delta-1)b_\omega(i)\right]}{(a_\delta-1)a_\omega(i)},i=2,3,...,n \tag{3}$$

This can be used to easily and quickly check the stability margin of the system after a disturbance[36]. By approximating $\Delta T'$ as the CCT[19,36], the coordinates of the critical stable operating point $(u_K^{cr},u_L^{cr},\delta_{KL}^{cr})$ and critical rate of the meta-generator l in the current system can also be estimated[37].

$$\begin{aligned}
u_i^{cr}&=\frac{a_u(i)}{2}\Delta T'^2+b_u(i)\Delta T'+c_u(i)\\
\delta_{KL}^{cr}&=b_{KL}\Delta T',\Delta t\in(0,\Delta T')\\
\delta_L{}^{cr}&=\frac{\arccos(\frac{|u_K|-|u_L|}{|2u_K|})-b_\delta}{a_\delta-1}=\frac{a_\omega(L)}{2}\Delta T'^2+b_\omega(L)\Delta T'+c_\omega(L)\\
\omega_L{}^{cr}&=\tan\frac{\delta_L{}^{cr}}{2}
\end{aligned} \tag{4}$$

In summary, the CCT and UEP can be calculated using only information about the rotation rate[12], but considering only a single information source may result in more errors. Theoretically, using $\Delta T'$ directly as the CCT would also lead to a conservative result. (Extended Data Table 1 can be referenced for more details)

The current power system is receiving an increasing number of renewable energy sources. These sources are connected to the power grid via inverters, which may change the inertia of the system[38–40], complicating the coefficients. This issue should be further studied.

On a finer scale, the operating points near the stability boundary exhibit unusual behavior (Figure 4).

Spontaneous synchronisation and boundary

a. $\sigma(\delta_i)$ is the standard deviation of δ. $\sigma(\delta_i)$ started to fall at 0.147s and rose by 1300% at 0.155s when the system became unstable.

b. In the $\delta_1-\delta_2$ plane, operating points appeared to cross the barrier before they reached the boundary. The elliptical area marks the position of the barrier. From 0.147s onwards the interval between operating points decreased in the direction of increasing Δt (shaded area).

c. In the u_1-u_2 plane, the graph is a critical state local attractor, which appears simultaneously with the synchronous barrier. The ellipse indicates the position of the attractor. The graph of the trajectory of the operating point from 0.147s onwards is shown as an attractor (in the shaded area).

As the stability boundary is approached, the perturbed trajectories of the operating points become interesting. The system self-organized and moved toward synchronous evolution[1].

The decrease in $\sigma(\delta_i)$ from the highest point indicated a tendency for the system to maintain its own stability before destabilizing and to spontaneously lead the velocities of the subsystems to the mean value. This may be the spontaneous synchronization effect caused by the coupling of the

Preprints (www.preprints.org) | NOT PEER-REVIEWED | Posted: 28 October 2023 doi:10.20944/preprints202310.1791.v1

systems (Figure 4). Spontaneous synchronization is precisely a self-organizing behavior, i.e., a phenomenon whereby initially unsynchronized coupled subsystems evolve toward synchronization[7,41]. Spontaneous synchronization seems to occur near the synchronization stability boundary (Extended Data Figure 7). For coupled network systems, this strong correlation indicates that the location where spontaneous synchronization occurs is also determined in $u_K - u_L - \delta_{KL}$ by Eq.1[1,20]. This may indicate that the mechanism of spontaneous synchronization is not necessarily related to the network topology, i.e., synchronization on the network may be independent of the network[42–44]. This will challenge the traditional perception of synchronization in networks. At the same time, the correlation may also indicate that physically, the synchronous stability boundary may originate from spontaneous synchronisation effects.

The generators spontaneously exchanged energy through coupling to synchronize and stabilize the system. This caused the coefficients in the fitted representation to change, which was reflected in the disturbed trajectory. When the conditions were correct ($\frac{d^2\delta_L}{d(\Delta t)^2} = a_\omega(i) < 0$ and a_δ is constant), a wonderful structure emerges from the trajectory of the operating points. Due to the constraint $\delta_K = a_\delta * \delta_L + b_\delta, \Delta t \in (0, \Delta T']$ and the same $\Delta T'$, the perturbed trajectories of all meta-generators simultaneously exhibit this structure. Although the phenomenon of self-organization of synchronization is often used directly to explain the synchronous operation of generators, this structure has rarely been reported in the past. The synchronous barrier and the cycle were the results of the self-organizing behavior in the $\delta_K - \delta_L$ and $u_K - u_L$ planes, respectively (Figure 4). The perturbed trajectory of the generator shows the same result at the same time (Extended Data Figure 3), proving that this is not caused by a substitution effect but by the emergent nature of the system at the boundary

After the operating point crosses the potential barrier, the energy is concentrated in a very short time in some of the generators, and $\sigma(\delta_i)$ rises sharply (Extended Data Figure 4). The operating point then crossed the boundary and destabilized the system.

This self-organization phenomenon on the boundary increases the error in the CCT and UEP. This will be explored further in the future.

The results of the self-organizing behavior are complex and do not always result in the formation of a synchronous potential barrier (Extended Data Figure 6). The reasons for this difference, or rather, the specific conditions for the formation of this particular structure of synchronized barrier, have yet to be investigated.

Conclusions

In this study, a graceful stabilizing boundary equation that accurately describes an ideal synchronous stabilizing boundary is derived. Since the physical quantities in the equation are independent of the network, it is universally applicable to almost any power network. Therefore, the synchronization stability of the grid can be analyzed in a uniform way. It is also shown in a seminal way that the mechanism of synchronization may not be linked to the network topology and parameters. The experimental data are derived from simulations of the IEEE standard arithmetic models. The self-organizing behavior at the operating point demonstrates the existence of spontaneous synchronization on the boundary of the synchronization stability domain, which helps to confirm the argument that spontaneous synchronization is directly equivalent to synchronization stability. Additionally, the self-organizing behavior suggests the existence of a new explanation for the origin of the grid synchronous stability boundary. The concise mathematical tools, simple and universal methods, and ability to assess synchronization stability by simply monitoring the voltage and angular velocity provide great convenience for engineering applications. It is also demonstrated that synchronous stability studies of other coupled systems without clear network details can be

Preprints (www.preprints.org) | NOT PEER-REVIEWED | Posted: 28 October 2023 doi:10.20944/preprints202310.1791.v1

performed by finding the correct parameters to directly derive the stability boundary while eliminating the need to construct elaborate network models. Thus, synchronization stability analyses in other disciplines may be able to directly apply the assumption made in the manuscript, with the exact form of Eq.1 depending on the form of the synchronous power and the coupling power in each discipline. Finally, the behavior of the real system's operating points near the boundary is still very complex. It is still difficult to accurately predict these results, such as the specific conditions and duration of the occurrence of synchronous barrier structures, which require further exploration.

Data availability: All the data that support the findings of this study are available at Figshare (DOI:10.6084/m9.figshare.23585961).

Conflicts of Interest: The author declare no conflicts of interest.

Extended Figure 1. Stability boundary for generators

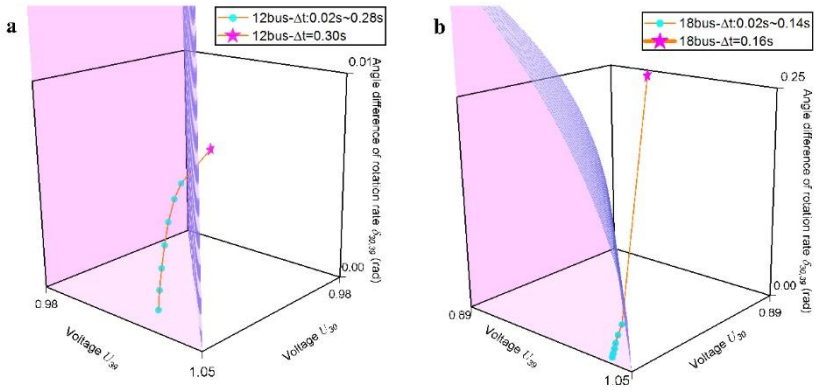

a and b correspond to IEEE 39-BUS system, generator disturbed instability process Schematic diagram of the disturbed trajectory of the operating point crossing the boundary after a three-phase short-circuit ground fault at 12bus and 18bus in node IEEE39 with gradually increasing Δt, respectively. (Δt increases from 0.04s, until destabilization)

Extended Figure 2. Fitting results for generator perturbed trajectories of 12bus after a three-phase short circuit to ground fault

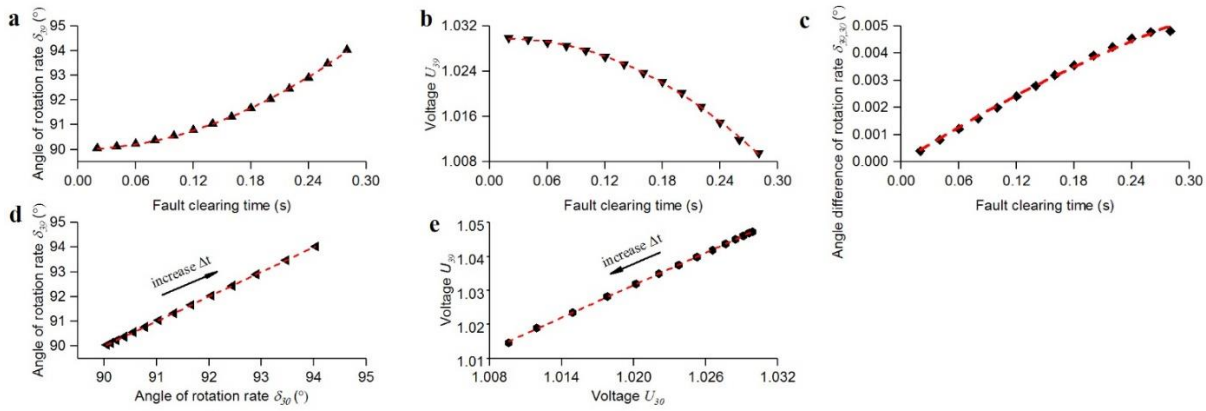

The expressions for the disturbed operating points of the meta-generators and generators have the same form before and after permutation.

a. The projection of the disturbed trajectory in the $\delta_{39}-\Delta t$ plane. The result of the fit is $\frac{a_\omega(1)}{2}=48.96109\pm0.79143, b_\omega(1)=0.52556\pm0.17753, c_\omega(1)=90$, and the adjusted R-squared value is 1.

Preprints (www.preprints.org) | NOT PEER-REVIEWED | Posted: 28 October 2023 doi:10.20944/preprints202310.1791.v1

b. The projection of the disturbed trajectory in the $u_{39}-\Delta t$ plane. The result of the fit is $\frac{a_u(1)}{2}=-0.2968\pm0.00968, b_u(1)=0.01069\pm0.00299$ and the adjusted R-squared value is 0.99905.

c. The projection of the disturbed trajectory in the $\delta_{39,30}-\Delta t$ plane. The result of the fit is $a_{12}=-0.01545\pm0.00238, b_{12}=0.02222\pm5.34533E\text{-}4$ and the adjusted R-squared value is 0.9993.

d. The projection of the disturbed trajectory in the $\delta_{30}-\delta_{39}$ plane. The result of the fit is $a_\delta=1.00019\pm3.59019E\text{-}4, b_\delta=-0.01749\pm0.03285$ and the adjusted R-squared value is 1.

e. The projection of the disturbed trajectory in the $u_{30}-u_{39}$ plane. The result of the fit is $a_v=1.59015\pm0.00611, b_v=-0.59037\pm0.00625$ and the adjusted R-squared value is 0.99981.

Extended Figure 3. IEEE 39-BUS system, self-organizing behavior of generators near the boundary

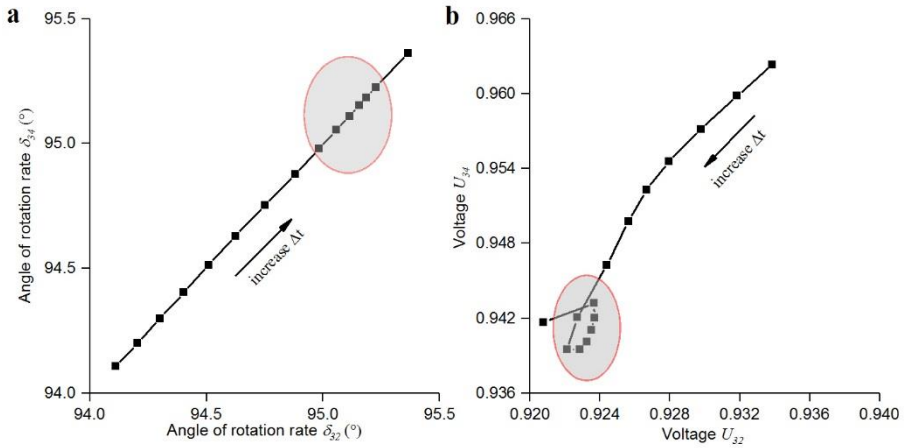

The 18bus three-phase short-circuit ground fault, increase in fault time Δt from 0.140s to 0.154s, and the trajectory of disturbed operating point near the boundary. The arrow shows the direction of increase of Δt. The generator has the same barrier and attractor as the meta-generator.

a. In the $\delta_{32}-\delta_{34}$ plane, running points appear to cross the barrier before they reach the boundary, and the elliptical area marks the position of the barrier. From 0.147s onwards the interval between running points decreases in the direction of increasing Δt

b. In the $u_{32}-u_{34}$ plane, the graph is presented as a critical state local attractor, which appears simultaneously with the synchronous barrier. The ellipse indicates the position of the attractor. The graph of the trajectory of the run point from 0.147s onwards is shown as an attractor (in the shaded area).

Extended Figure 4. Stability boundary for meta-generators for IEEE 9-BUS system

Preprints (www.preprints.org) | NOT PEER-REVIEWED | Posted: 28 October 2023 doi:10.20944/preprints202310.1791.v1

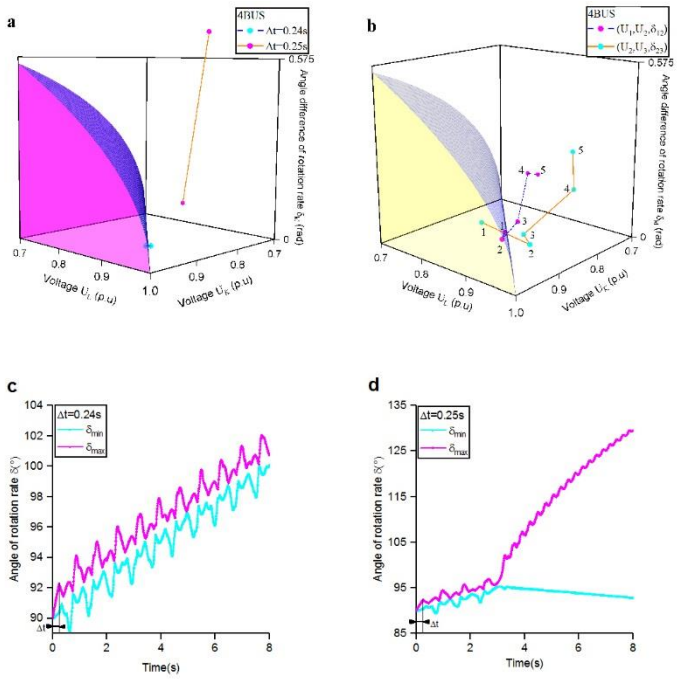

a. The same boundary equation applise to the 3-machine 9-node system. 4bus sets the location of the operating point after a three-phase short-circuit ground fault.

b. Results of the multiswing instability for Δt=0.25s.

c and d are the results of the 4BUS three-phase ground fault simulation, respectively. It is stable at $\Delta t = 0.24s$, unstable at $\Delta t = 0.25s$, and unstable in $(3s,4s)$.

Extended Figure 5. Fitting results for meta-generator perturbed trajectories of 4bus after a three-phase short circuit to ground fault

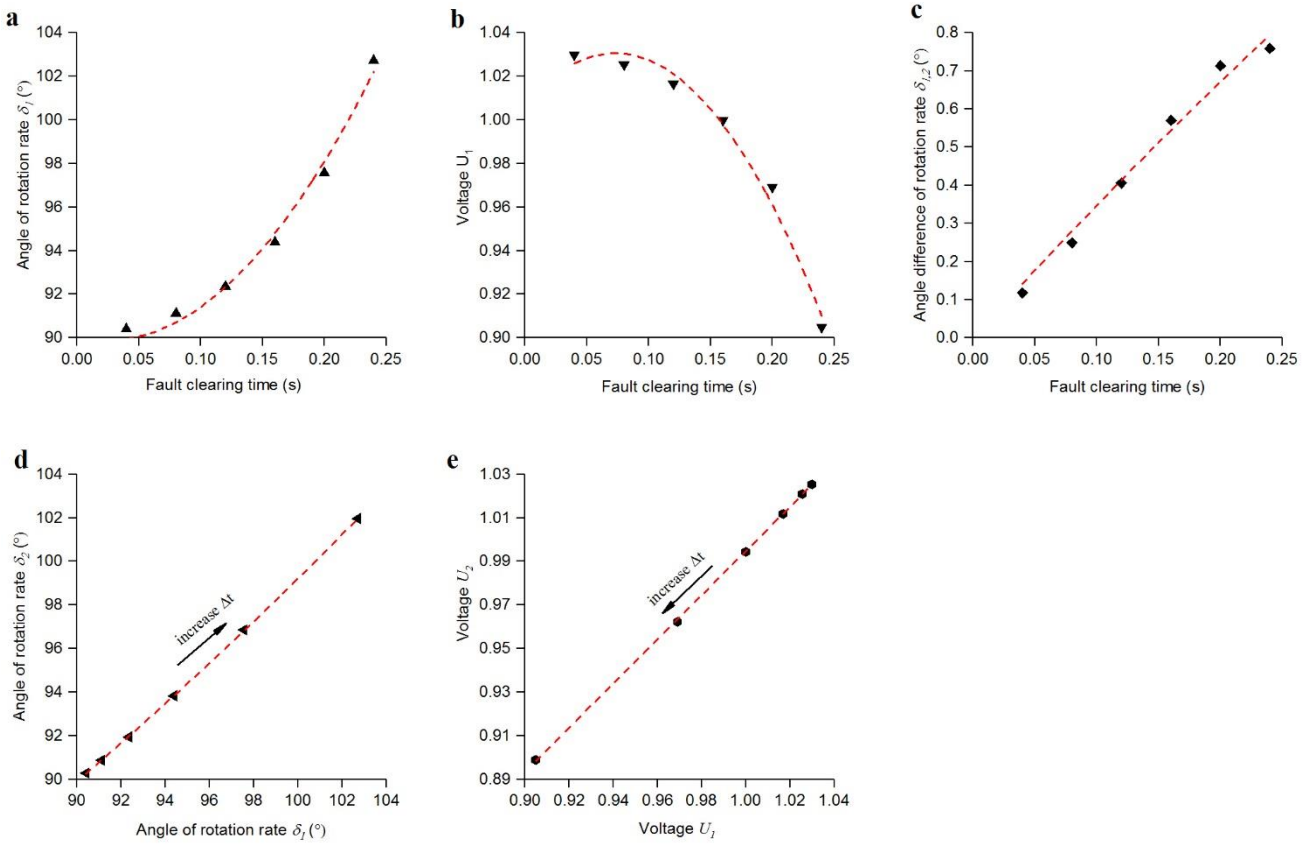

Preprints (www.preprints.org) | NOT PEER-REVIEWED | Posted: 28 October 2023 doi:10.20944/preprints202310.1791.v1

Fitting results for perturbed trajectories for the 4bus trajectory of disturbed operating points after a three-phase short-circuit ground fault..

a. The projection of the disturbed trajectory in the $\delta_1 - \Delta t$ plane. The result of the fit is $\frac{a_\omega(1)}{2} = 263.16677 \pm 27.27487, b_\omega(1) = -12.16449 \pm 5.45497, c_\omega(1) = 90$. The adjusted R-squared value is 0.99997.

b. The projection of the disturbed trajectory in the $u_1 - \Delta t$ plane. The result of the fit is $\frac{a_u(1)}{2} = -4.32887 \pm 0.74225, b_u(1) = 0.63292 \pm 0.21231, c_u(1) = 1.00743 \pm 0.01298$, and the adjusted R-squared value is 0.97679.

c. The projection of the disturbed trajectory in the $\delta_{12} - \Delta t$ plane. The result of the fit is $a_{12} = -0.01956 \pm 0.03364, b_{12} = 0.06242 \pm 0.00673$, and the adjusted R-squared value is 0.99519.

d. The projection of the disturbed trajectory in the $\delta_1 - \delta_2$ plane. The result of the fit is $a_\delta = 1.05168 \pm 0.01287, b_\delta = -4.40363 \pm 1.21501$, and the adjusted R-squared value is 0.99925.

e. The projection of the disturbed trajectory in the $u_1 - u_2$ plane. The result of the fit is $a_\nu = 0.98731 \pm 0.00722, b_\nu = 0.01791 \pm 0.00713$, and the adjusted R-squared value is 0.99973.

Extended Figure 6. Spontaneous synchronization behaviour of running points near the boundary

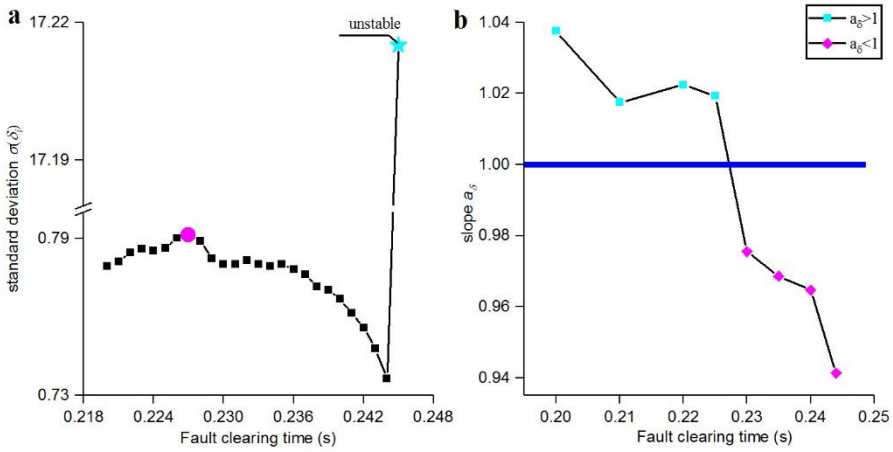

a. The standard deviation of δ decreases from Δt=0.227s. It rises by 2200% at Δt=0.245s, where there is an instability.

b. Derive $\frac{d\delta_{kl}}{d(\Delta t)} = \frac{d((a_\delta - 1)\delta_l + b_\delta)}{d(\Delta t)} = (a_\delta - 1) * \frac{d\delta_l}{d(\Delta t)}$ from the fitted equation (e). Due to the monotonicity of δ_i with respect to Δt, i.e. $\frac{d\delta_l}{d(\Delta t)} > 0, \Delta t \in (0, CCT)$, $a_\delta - 1$ changes from positive to negative and a_δ changes from greater than 1 to less than 1.

Extended Figure 7. IEEE 39bus system, Spontaneous synchronisation always occurs near the synchronisation stability boundary

Preprints (www.preprints.org) | NOT PEER-REVIEWED | Posted: 28 October 2023 doi:10.20944/preprints202310.1791.v1

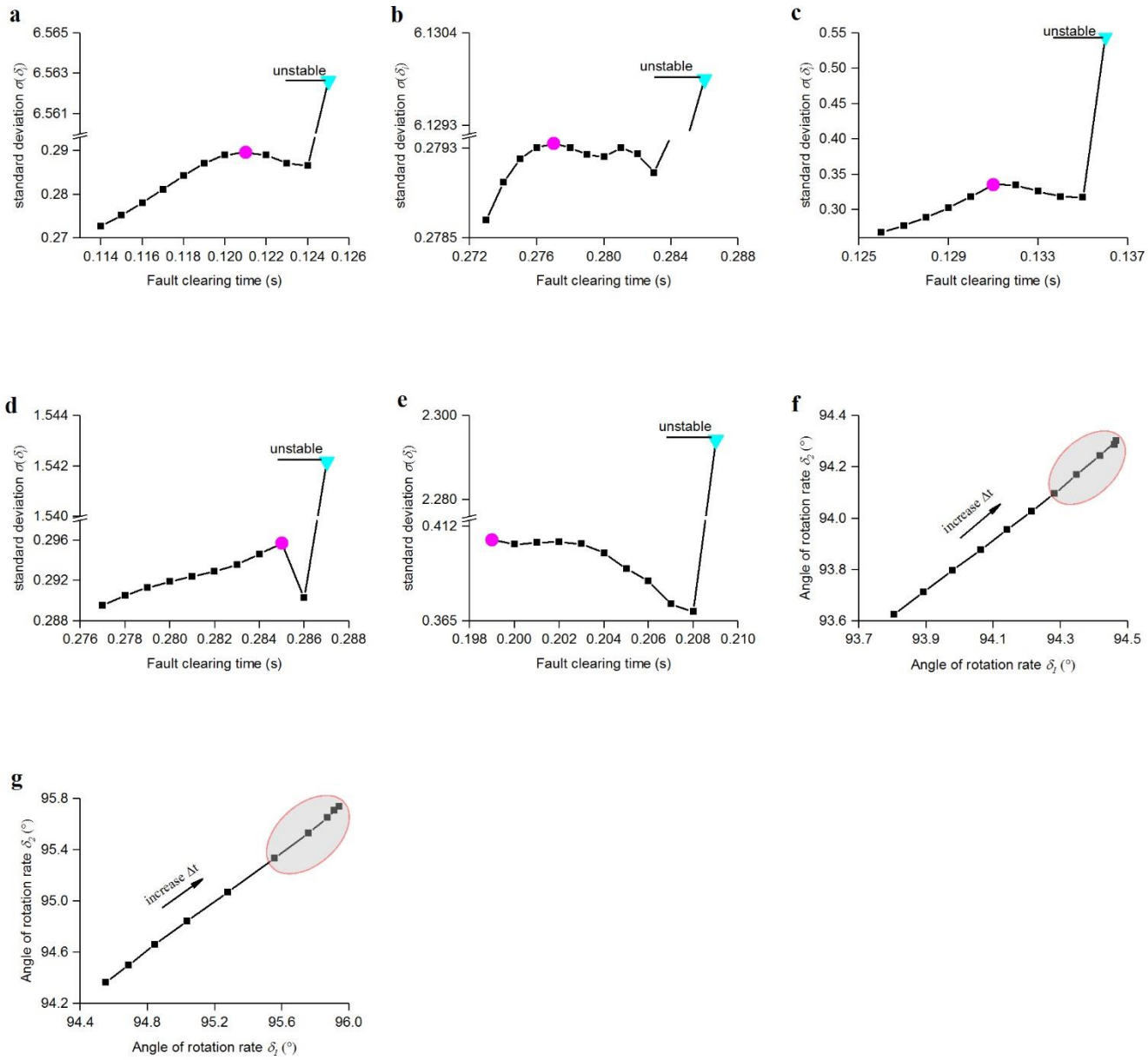

A three-phase short-circuit ground fault is set at the corresponding node. a, b, c, d, e correspond to the critical behaviour of the operating points after the failure of 6bus, 12bus, 24bus, 30bus & 36bus respectively. All the results show that near the boundary, there is always a significant decrease in $\sigma(\delta_i)$. These results demonstrate a strong correlation between synchronisation stability boundary and spontaneous synchronisation.

f and g show that the behaviour of the operating points also show the phenomenon of synchronous barrier when faults are set at 6bus and 24bus (shaded area).

References

1. Motter, A. E., Myers, S. A., Anghel, M. & Nishikawa, T. Spontaneous synchrony in power-grid networks. *Nat. Phys.* **9**, 191–197 (2013).
2. Yu, Y., Liu, Y., Qin, C. & Yang, T. Theory and Method of Power System Integrated Security Region Irrelevant to Operation States: An Introduction. *Engineering* **6**, 754–777 (2020).
3. Yang, P., Liu, F., Wei, W. & Wang, Z. Approaching the Transient Stability Boundary of a Power System: Theory and Applications. *IEEE Trans. Autom. Sci. Eng.* 1–12 (2022) doi:10.1109/TASE.2022.3213678.
4. Molnar, F., Nishikawa, T. & Motter, A. E. Asymmetry underlies stability in power grids. *Nat. Commun.* **12**, 1–9 (2021).

5. Martínez, I., Messina, A. R. & Vittal, V. Normal form analysis of complex system models: A structure-preserving approach. *IEEE Trans. Power Syst.* **22**, 1908–1915 (2007).
6. Bhui, P. & Senroy, N. Real-Time Prediction and Control of Transient Stability Using Transient Energy Function. *IEEE Trans. Power Syst.* **32**, 923–934 (2017).
7. Zhu, L. & Hill, D. J. Synchronization of Kuramoto Oscillators: A Regional Stability Framework. *IEEE Trans. Automat. Contr.* **65**, 5070–5082 (2020).
8. Koronovskii, A. A., Moskalenko, O. I. & Hramov, A. E. synchronization in complex networks. *Tech. Phys. Lett.* **38**, 924–927 (2012).
9. Casals, M. R. *et al.* Knowing power grids and understanding complexity science. *Int. J. Crit. Infrastructures* **11**, 4 (2015).
10. Gurrala, G., Dimitrovski, A., Pannala, S., Simunovic, S. & Starke, M. Parareal in Time for Fast Power System Dynamic Simulations. *IEEE Trans. Power Syst.* **31**, 1820–1830 (2016).
11. Gurrala, G. *et al.* Large Multi-Machine Power System Simulations Using Multi-Stage Adomian Decomposition. *IEEE Trans. Power Syst.* **32**, 3594–3606 (2017).
12. Wang, B., Fang, B., Wang, Y., Liu, H. & Liu, Y. Power System Transient Stability Assessment Based on Big Data and the Core Vector Machine. *IEEE Trans. Smart Grid* **7**, 2561–2570 (2016).
13. Al-Ammar, E. A. & El-Kady, M. A. Application of operating security regions in power systems. *IEEE PES Transm. Distrib. Conf. Expo. Smart Solut. a Chang. World* (2010) doi:10.1109/TDC.2010.5484270.
14. Kundur, P. *et al.* Definition and classification of power system stability. *IEEE Trans. Power Syst.* **19**, 1387–1401 (2004).
15. Student Member, B. B. & Senior Member, G. A. On the nature of unstable equilibrium points in power systems. *IEEE Trans. Power Syst.* **8**, 738–745 (1993).
16. Chiang, H. D., Wu, F. F. & Varaiya, P. P. A BCU Method for Direct Analysis of Power System Transient Stability. *IEEE Trans. Power Syst.* **9**, 1194–1208 (1994).
17. Shubhanga, K. N. & Kulkarni, A. M. Application of Structure Preserving Energy Margin Sensitivity to Determime the Effectiveness of Shunt and Serles FACTS Devices. *IEEE Power Eng. Rev.* **22**, 57 (2002).
18. Al Marhoon, H. H., Leevongwat, I. & Rastgoufard, P. A fast search algorithm for Critical Clearing Time for power systems transient stability analysis. *2014 Clemson Univ. Power Syst. Conf. PSC 2014* (2014) doi:10.1109/PSC.2014.6808093.
19. Rimorov, D., Wang, X., Kamwa, I. & Joos, G. An approach to constructing analytical energy function for synchronous generator models with subtransient dynamics. *IEEE Trans. Power Syst.* **33**, 5958–5967 (2018).
20. Dörfler, F., Chertkov, M. & Bullo, F. Synchronization in complex oscillator networks and smart grids. *Proc. Natl. Acad. Sci. U. S. A.* **110**, 2005–2010 (2013).
21. Cuadra, L., Salcedo-Sanz, S., Del Ser, J., Jiménez-Fernández, S. & Geem, Z. W. A critical review of robustness in power grids using complex networks concepts. *Energies* **8**, 9211–9265 (2015).
22. Zhou, J. *et al.* Large-Scale Power System Robust Stability Analysis Based on Value Set Approach. *IEEE Trans. Power Syst.* **32**, 4012–4023 (2017).
23. Ajala, O., Dominguez-Garcia, A., Sauer, P. & Liberzon, D. A Second-Order Synchronous Machine Model for Multi-swing Stability Analysis. *51st North Am. Power Symp. NAPS 2019* (2019) doi:10.1109/NAPS46351.2019.9000368.
24. Karatekin, C. Z. & Uçak, C. Sensitivity analysis based on transmission line susceptances for congestion management. *Electr. Power Syst. Res.* **78**, 1485–1493 (2008).
25. Mei, S., Ni, Y., Wang, G. & Wu, S. A study of self-organized criticality of power system under cascading failures based on AC-OPF with voltage stability margin. *IEEE Trans. Power Syst.* **23**, 1719–1726 (2008).
26. Dobson, I., Carreras, B., Lynch, V. & Newman, D. An initial model for complex dynamics in electric power system blackouts. *Proc. Hawaii Int. Conf. Syst. Sci.* 51 (2001) doi:10.1109/hicss.2001.926274.
27. Ding, L., Gonzalez-Longatt, F. M., Wall, P. & Terzija, V. Two-step spectral clustering controlled islanding algorithm. *IEEE Trans. Power Syst.* **28**, 75–84 (2013).
28. Znidi, F., Davarikia, H. & Rathore, H. Power Systems Transient Stability Indices: Hierarchical Clustering Based Detection of Coherent Groups Of Generators. (2021).
29. Kuramoto, Y. & Battogtokh, D. Coexistence of Coherence and Incoherence in Nonlocally Coupled Phase Oscillators. *Physics (College. Park. Md).* **4**, 380–385 (2002).
30. Martens, E. A., Thutupalli, S., Fourrière, A. & Hallatschek, O. Chimera states in mechanical oscillator networks. *Proc. Natl. Acad. Sci. U. S. A.* **110**, 10563–10567 (2013).

31. Panaggio, M. J. & Abrams, D. M. Chimera states: Coexistence of coherence and incoherence in networks of coupled oscillators. *Nonlinearity* **28**, R67–R87 (2015).
32. Amirthalingam, K. M. & Ramachandran, R. P. Improvement of transient stability of power system using solid state circuit breaker. *Am. J. Appl. Sci.* **10**, 563–569 (2013).
33. Liu, X., Shahidehpour, M., Cao, Y., Li, Z. & Tian, W. Risk assessment in extreme events considering the reliability of protection systems. *IEEE Trans. Smart Grid* **6**, 1073–1081 (2015).
34. Huang, R. *et al.* Learning and Fast Adaptation for Grid Emergency Control via Deep Meta Reinforcement Learning. *IEEE Trans. Power Syst.* **37**, 4168–4178 (2022).
35. Guo, M., Xu, D. & Liu, L. Design of Cooperative Output Regulators for Heterogeneous Uncertain Nonlinear Multiagent Systems. *IEEE Trans. Cybern.* **52**, 5174–5183 (2022).
36. Roberts, L. G. W., Champneys, A. R., Bell, K. R. W. & Di Bernardo, M. Analytical Approximations of Critical Clearing Time for Parametric Analysis of Power System Transient Stability. *IEEE J. Emerg. Sel. Top. Circuits Syst.* **5**, 465–476 (2015).
37. Owusu-Mireku, R., Chiang, H. D. & Hin, M. A Dynamic Theory-Based Method for Computing Unstable Equilibrium Points of Power Systems. *IEEE Trans. Power Syst.* **35**, 1946–1955 (2020).
38. Sajadi, A., Kenyon, R. W. & Hodge, B. M. Synchronization in electric power networks with inherent heterogeneity up to 100% inverter-based renewable generation. *Nat. Commun.* **13**, 1–12 (2022).
39. Sun, M. *et al.* On-line power system inertia calculation using wide area measurements. *Int. J. Electr. Power Energy Syst.* **109**, 325–331 (2019).
40. Zhang, Y., Bank, J., Muljadi, E., Wan, Y. H. & Corbus, D. Angle instability detection in power systems with high-wind penetration using synchrophasor measurements. *IEEE J. Emerg. Sel. Top. Power Electron.* **1**, 306–314 (2013).
41. Dörfler, F. & Bullo, F. Synchronization in complex networks of phase oscillators: A survey. *Automatica* **50**, 1539–1564 (2014).
42. Chen, G. Searching for Best Network Topologies with Optimal Synchronizability: A Brief Review. *IEEE/CAA J. Autom. Sin.* **9**, 573–577 (2022).
43. Li, X., Wei, W. & Zheng, Z. Promoting synchrony of power grids by restructuring network topologies. *Chaos An Interdiscip. J. Nonlinear Sci.* **33**, 63149 (2023).
44. Zhang, Y. & Motter, A. E. Symmetry-Independent Stability Analysis of Synchronization Patterns. *SIAM Rev.* **62**, 817–836 (2020).